Terrestrial Laser Scanning of Swiss subalpine forest for radiative transfer modelling

Matthew Purslow & Steven Hancock

13th October 2023

NERC GEF Loan 1114 Scientific Report

Abstract

Vegetation structure has a significant impact on snow modelling. Here, we surveyed a subalpine forest used for snow-forest interaction research in Davos, Switzerland through Terrestrial Laser Scanning (TLS). By voxelising the TLS data, we produce a three dimensional map of gap fraction that we use to drive the shadowVox radiative transfer model. These model runs will be used in future to evaluate the accuracy of shadowVox simulations of in-situ radiance measurements, optical satellite surface reflectance retrievals and satellite lidar measurements.

1 Background

Snow cover has a significant impact on the Earth's radiative budget (Gulev et al., 2021). This is due to snow having a high albedo relative to other terrestrial surfaces. Modelling of interactions between radiation, snow and forest canopies are required to quantify the impact of snow on the albedo of forested regions (Essery, 2013). The shortwave radiation budget of forest snowpacks at meter scale is predominantly controlled by canopy shading (Malle et al., 2019). The propagation of radiation through forest canopies is highly variable due to the heterogeneity of forest structure; this causes variability in the radiative budget of below-canopy snow. Parameterisation of these small-scale radiative processes within global climate models could contribute to improved projections of future snow-albedo interactions (Ni-Meister and Gao, 2011).

The aim of this survey was to collect a large continuous Terrestrial Laser Scanning (TLS) plot in an area of subalpine forest with a diversity of tree ages and stand geometries. This was then used to build voxel scenes for the shadowVox radiative transfer model (Hancock, in prep). shadowVox offers a fast, efficient method for modelling shortwave radiative transfer through forest canopies; model scenes are built through the voxelisation of TLS data into three dimensional maps of gap fraction.

The forest at Laret, Davos, Switzerland (Figure 1, 9.875 °E, 46.845 °N) has been used for a number of previous and ongoing forest-snow interaction studies (e.g. Webster et al., 2016; Malle et al., 2019; Mazzotti et al., 2021). While the survey was being undertaken, weather station and radiometer measurements were being collected alongside regular snow pit measurements. The site is an example of a forest managed by selective harvesting, constituted primarily of Norway Spruce with smaller populations of pine and larch. The selective harvesting practice means that the trees at Laret range from saplings to fully-matured trees.

The survey was undertaken using the equipment described in Table 1 during March 2022; this was the beginning of the local snowmelt season (Tobias Jonas, personal communication). The snow suppressed the understorey such that the survey measured trees but not shrubs. Snow melt meant that the snow depth changed over the course of the month. However, the ground remained snow-covered throughout with the exception of some bare patches at the base of exposed trees in the final week.

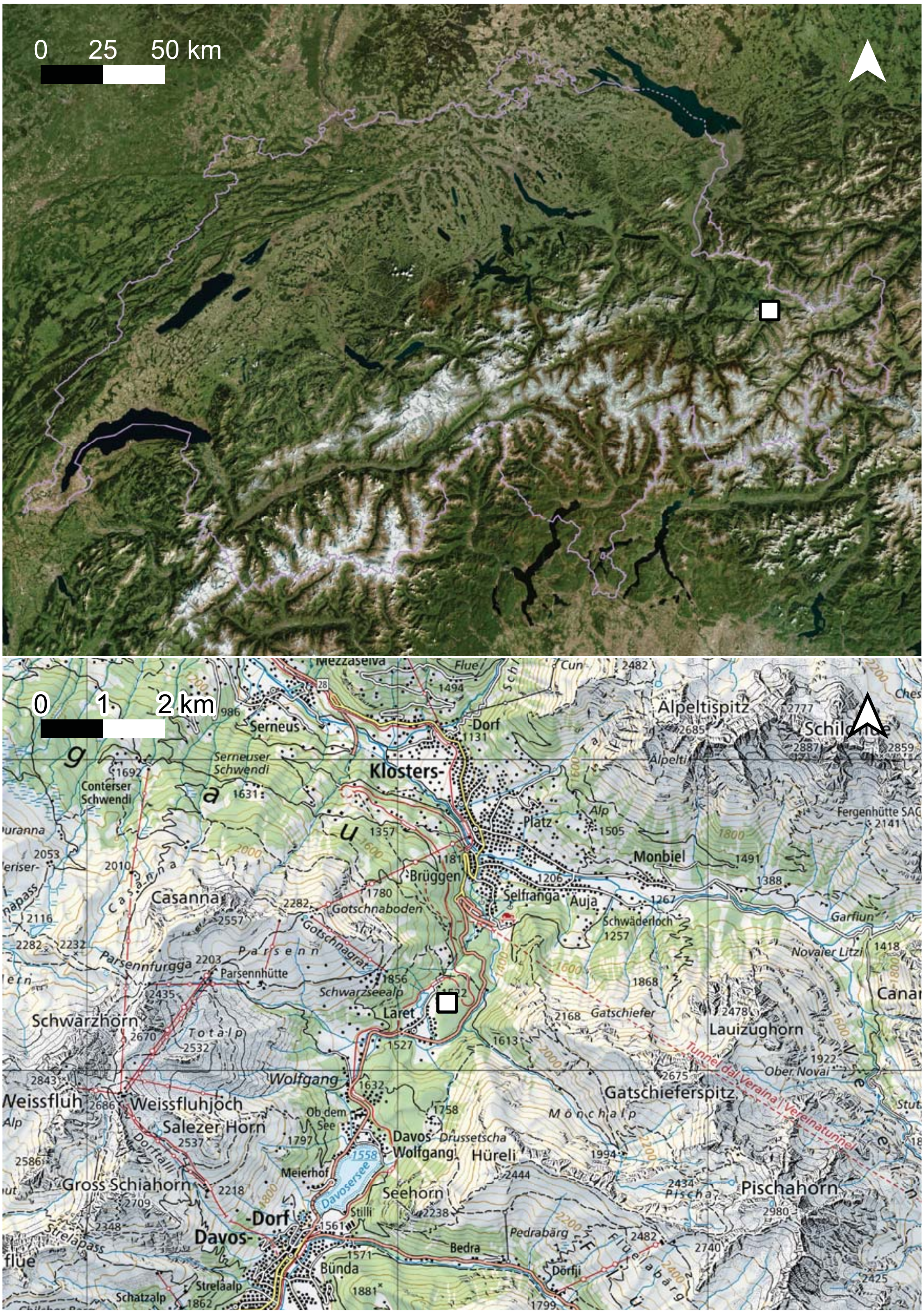

Figure 1: Field survey site location (9.875 °E, 46.845 °N) in Laret, Davos, Switzerland (white box). Top panel shows site location within Switzerland and bottom panel shows site location within Davos-Klosters. Satellite imagery and map provided by the Swiss Federal Office of Topography (© swisstopo).

Table 1: List of equipment used, with quantity and provider. NERC GEF = Natural Geophysical Equipment Facility, WSL = Eidgenossische Forschungsanstalt fur Wald, Schnee und Landschaft (Swiss Federal Institute for Forest, Snow and Landscape Research), SLF = Institut fur Schnee- und Lawinenforschung (Institute for Snow and Avalanche Research).

Item	Quantity	Serial Number(s)	Provider
Riegl VZ-1000 Laser Scanner & accessories	1	S9999556	NERC GEF
Lenovo P50 Laptop & accessories	1	PC0K6QF9	NERC GEF
RiScan Pro Software v2.1	1		NERC GEF
RiScan Pro Dongle	1		NERC GEF
Leica GS10 GNSS Receivers & accessories	2	1534766, 1535178	NERC GEF
Tilt and Turn Targets Retro Reflective	6		NERC GEF
Reflective targets	28		Steven Hancock
Survey tripods	3		WSL/SLF
Prism poles	4		WSL/SLF
Garden stakes (2.8m)	32		WSL/SLF

2 Survey procedure

2.1 Geolocation

Global Navigation Satellite System (GNSS) base and rover stations were used to geolocate the survey. A reference point was established by marking a short fence post near to the access point for the field site with a clear view of much of the sky; the GNSS base station was established directly over this pin. Tilt-and-turn targets were placed on a tripod and 4 prism poles spread across the two largest clearings within the plot, all visible from the intended first scan position while being at a range of elevations. Screw-to-stub adapters were used to allow for easy exchange of targets with the GNSS rover antenna. Target positions were measured using the rover, working anticlockwise and beginning and ending at the same target. The rover was left at the first target position for extended periods before and after surveying the other target locations, which were themselves measured for five minutes each.

2.2 Rolling target workflow

Before beginning the TLS survey, targets were distributed in the south-western corner of the field site. Targets were not placed on a regular grid. Instead, we aimed to maximise the number of viable scan positions with line of sight to each target. The field site was accessible to the public, and so it was requested by our partners at the Institute for Snow and Avalanche Research (SLF) that we minimise the footprint of our survey when we were not present at the site. We therefore spread the targets across an approximately 50×50 m area to begin. Once this area was scanned, targets near the center of this area were rolled north-eastwards, with targets at or near the boundary remaining to act as tiepoints for the next set of scans.

Our first TLS position was at the high point of the clearing in the west of the survey area (Figure 2), with clear line of sight to all tilt-and-turn targets. This ensured that the survey could be geolocated accurately. At this position, and all subsequent positions, the following procedure was followed:

- Set up tripod (relatively level) with tilt mount attached
- Unpack, affix TLS upright and power up
- Measure snow depth of undisturbed snow near tripod position
- Run quick scan to find tie points
- Scan tie points

- While scanning, take photographs to north, east, south, west and upwards from scan position
- Register the scan to ensure a sufficient number of targets are visible
- Run full scan at 0.018° resolution with 400 m range (approximately five minutes)
- If canopy tops were not visible in the first scan, tilt scanner to horizontal and repeat scans

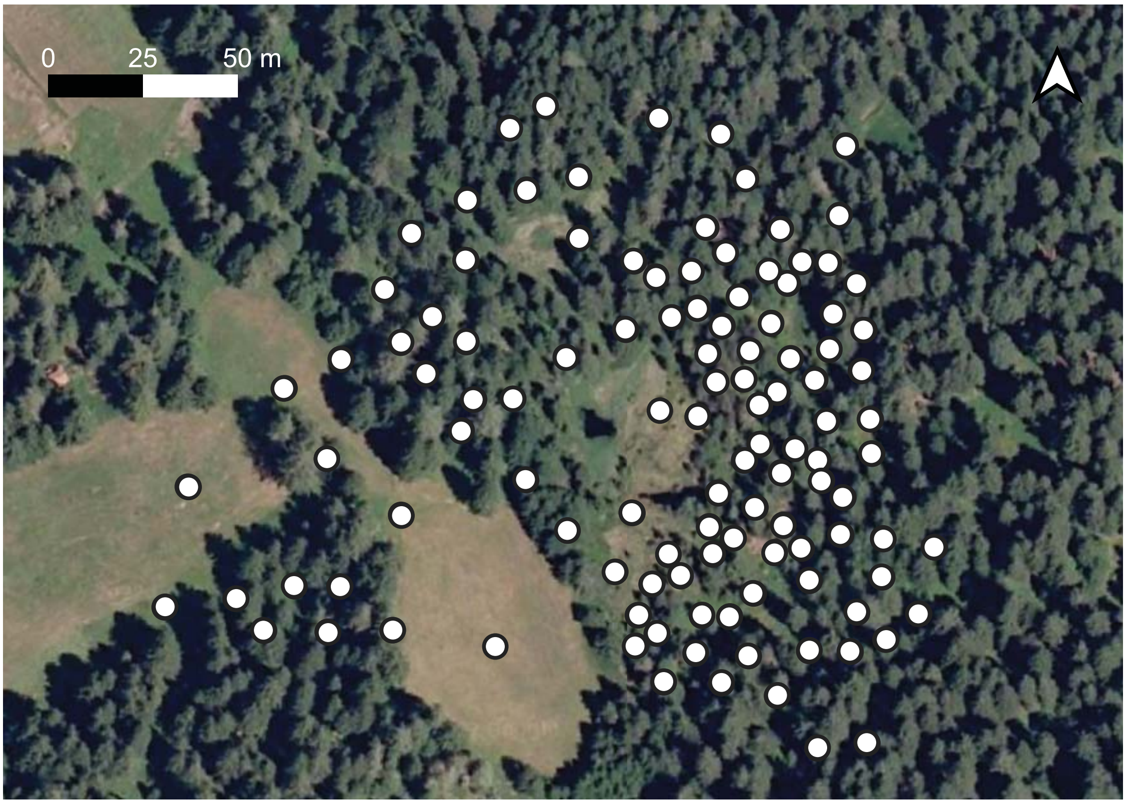

Figure 2: Scan locations within field site at Laret, Davos, Switzerland. Aerial imagery provided by the Swiss Federal Office of Topography (© swisstopo).

At the end of each field day, all data collected was backed up to a hard drive and to The University of Edinburgh DataStore. TLS scans registered during the day were assessed visually for the accuracy of the registration. At several intervals through the campaign, the data was processed using voxelate (Steven Hancock, 2021) to visualise occlusion (Figure 3) and ensure that the data collected was of sufficient quality. Quality was assessed by determining the stability of the within voxel gap fraction for different combinations of TLS scans, as a function of occlusion from the scans to that voxel. This revealed that, as long as at least one TLS scan position has at less than 60% occlusion to a voxel, that voxel will have a stable gap fraction (and so plant area) estimate. A paper describing this test is in preparation.

2.3 Recommendations for future borrowers

Rolling targets meant that a large continuous area could be surveyed without a correspondingly large number of targets. Target movement through the course of the survey due to melting snow was mitigated by ensuring target poles were inserted as deep as possible and into soil where possible (a snow shovel was used if necessary). If the survey were repeated, we would georeference the survey after the first day to assist with future planning and data visualisation. Additionally, using markers to stake out segments of the larger plot would have ensured a more uniform survey geometry.

The number of scans within the survey proved problematic from a computing perspective. By the final week, the survey exceeded the 500GB capacity of the laptop being used in the field. This necessitated the removal of coarse-resolution scans that were used to find targets from the survey.

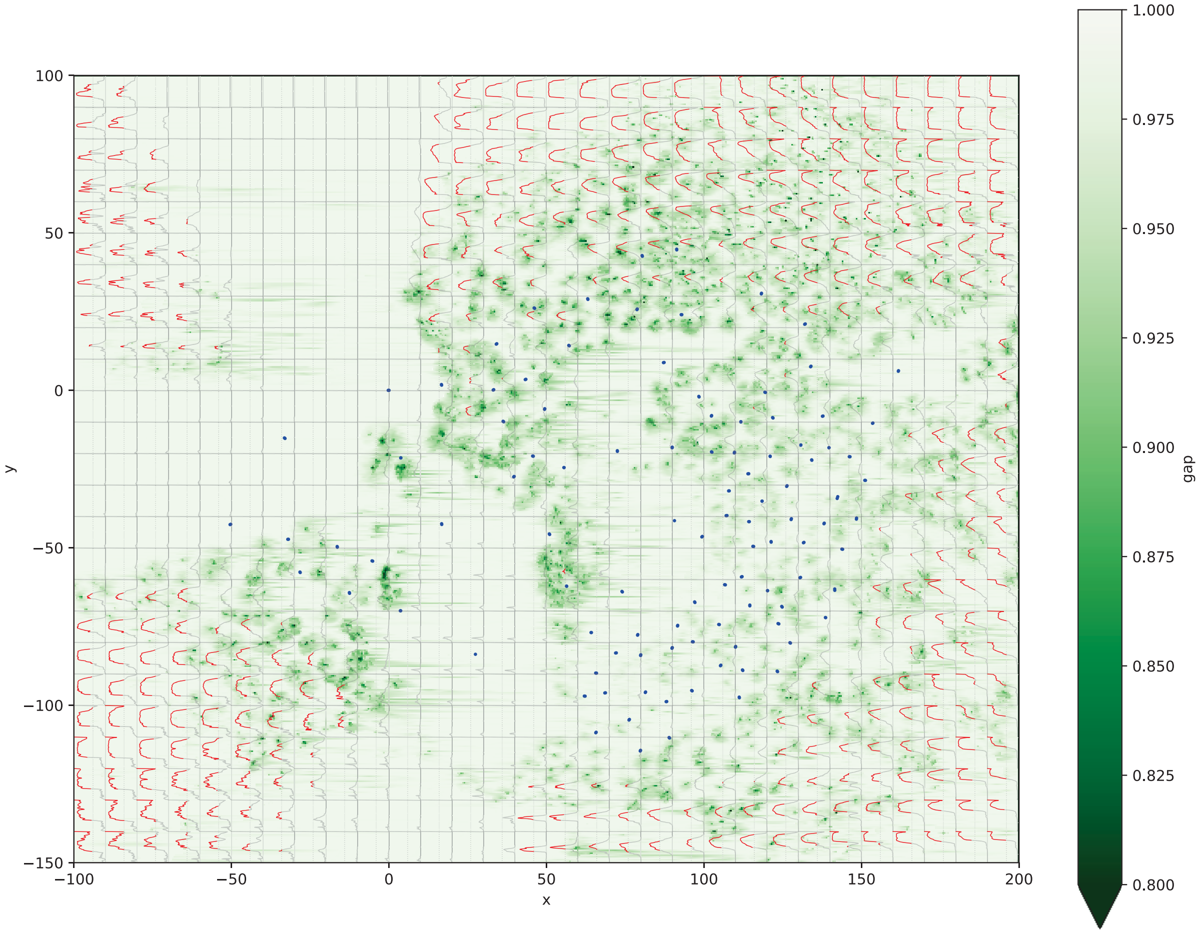

Figure 3: Example map of voxel occlusion within the survey for data collected before 25th March 2022. Blue dots indicate scan positions. Green shows the mean gap fraction for each column of $0.5\times0.5\times0.5$ m voxels. For each 10×10 m grid square, the mean fraction of beams reaching the voxels at that height is plotted and coloured red where the fraction is lower than 0.6.

Final processing was undertaken in the UK on a different laptop with greater storage. We would recommend using a laptop with significantly larger storage if undertaking surveys of a similar size in future (e.g 2TB).

For gap fraction based methods, assessing the occlusion at regular intervals throughout data collection (Figure 3) can show where additional scan positions are needed. The code used during this study, designed to work with the raw Riegl outputs, is available open-source (Steven Hancock, 2021).

3 Data quality

The TLS scan pattern was at a fairly fine resolution (0.018°×0.018°). This ensured that voxels were intersected by many beams, improving the reliability of gap fraction estimates. Figure 4 shows the facing view from Scan Position 48, which was collected in the center of the clearing being monitored by cablecar- and ground-based radiometers during the survey. In general, wind speeds were low, minimising the movement of trees during and between scans. However, because the intended use of this data was for voxelisation, the suitability of the data for quantitative structural modelling (e.g. Hackenberg et al., 2015) is unknown.

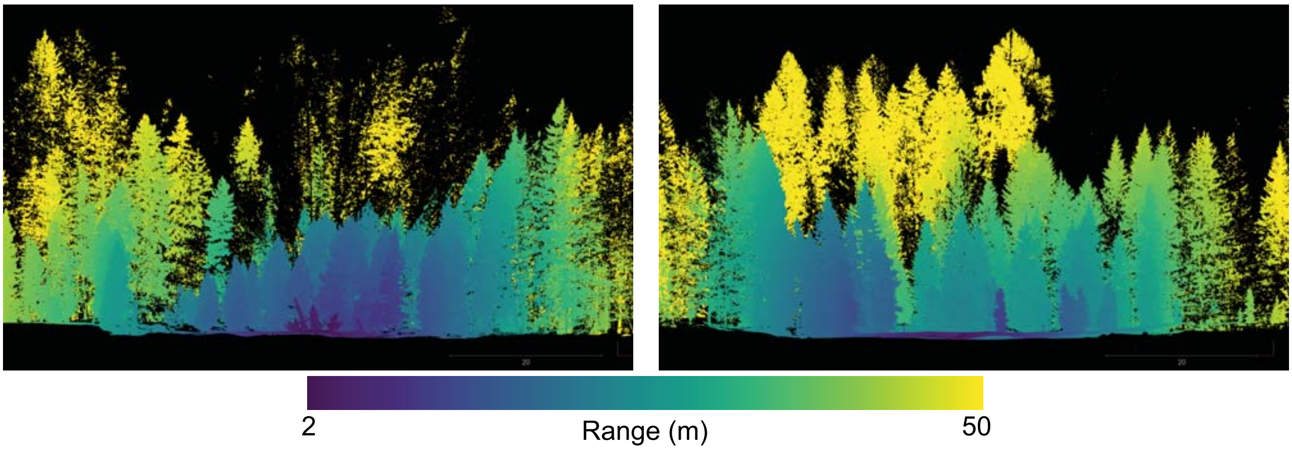

Figure 4: Example point cloud from Scan Position 48, north (left) and south (right) of the scan position. Colourised by range from the scanner.

4 Processing and modelling

4.1 Geolocation data

GNSS measurements were process following the protocol provided by GEF using Leica Infinity. Position data from the Automated GNSS Network for Switzerland (AGNES) station DAV2 (usefully situated on the hillside above the SLF office in Davos) was used to improve the base station location accuracy. Rover measurements of tilt-and-turn target locations were processed to get their positions relative to the base station and these positions were then identified in the TLS data.

4.2 TLS data

TLS data was processed in RiSCAN Pro 2.1. After registering the scans using tie points, we ran the default multistation adjustment with planes to improve the scan alignment. The scans were then georeferenced using the GNSS survey output for the tilt-and-turn targets.

Once geolocated, the TLS data has been processed using voxelate (Steven Hancock, 2021) to produce $50 \times 50 \times 50$ cm voxel maps of gap fraction and Plant Area Index (PAI). These voxel maps can then be used as radiative transfer model scenes for shadowVox. This process is based on the beam geometry as recorded by the scanner as opposed to the point cloud commonly used as output from TLS surveys.

5 Preliminary findings & interpretation to date

Figure 5 shows example output from shadowVox using the data collected at Laret. It shows that the model replicates the expected spatial distribution of shadows cast by trees at a resolution useful to high-resolution snow modelling research. Future work will assess the accuracy of these sub-canopy insolation measurements against in-situ measurements. These results suggest that TLS-derived voxel scenes offer an efficient route to modelling the light regimes of subalpine forests.

Figure 6 shows a comparison of a Bing aerial image (www.bing.com/maps) with an above canopy reflectance simulation from the TLS voxels. Note that the ground is treated as snow in the simulation. The next step will be to quantitatively validate this simulation against Sentinel-2 data. Note the loss of detail due to occlusion at the right of the simulated image. This is outside of the field plot.

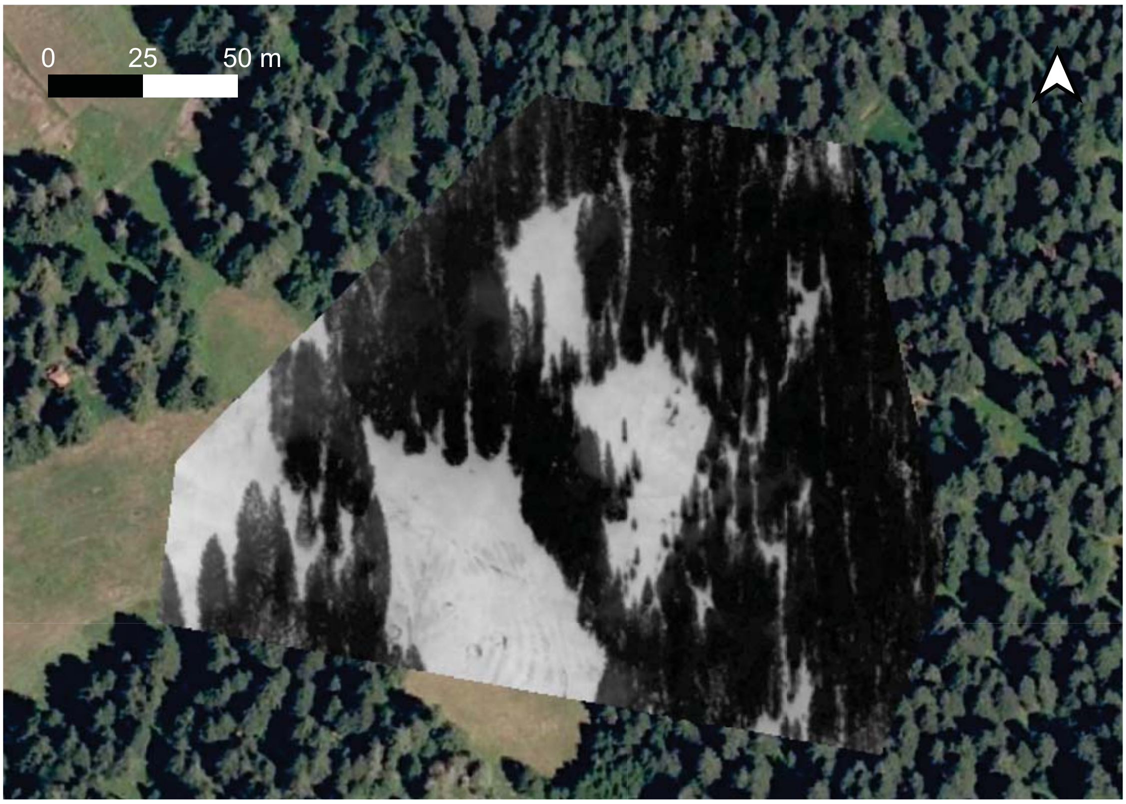

Figure 5: Example output from shadowVox, showing terrain insolation for 45° solar zenith angle and 180° solar azimuth angle, overlaid on aerial imagery for the site provided by the Swiss Federal Office of Topography (© swisstopo).

6 Conclusions and recommendations

We performed a large Terrestrial Laser Scanning survey of subalpine forest in Davos, Switzerland. The data collected was successfully used to build voxel scenes of gap fraction as input into the shadowVox radiative transfer model. Model output aligns well with expected patterns of shading in the forest. Future work will directly validate shadowVox against in-situ radiometry measurements (after Malle et al., 2019) and satellite-derived surface reflectance measurements.

Repeated assessment of occlusion through the course of the survey was beneficial. By mapping the level of occlusion from scans undertaken up to a certain date, future scan and target placement could adapt to ensure that the data collected was of sufficient quality for radiative transfer modelling. The occlusion mapping is available in the voxelate package (Steven Hancock, 2021).

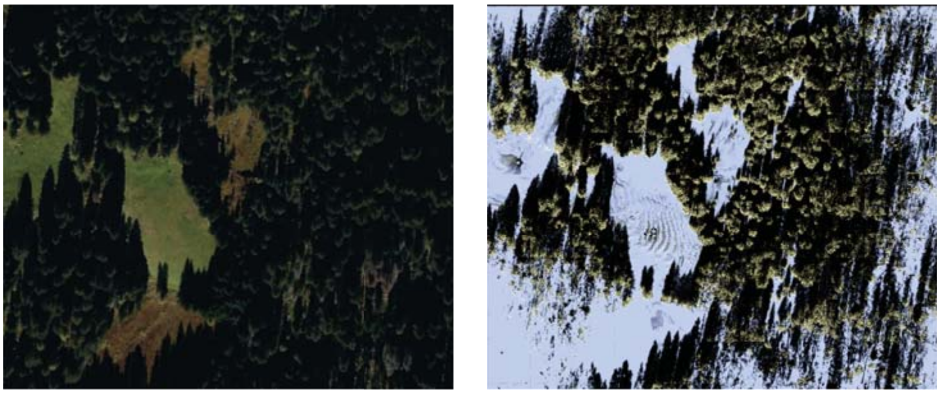

Figure 6: Comparison of an RGB image of Laret from Bing (on left, in summer) and for similar lighting conditions from the shadowVox (on right, in winter)

The scale of the survey was limited by the requirement to fine scan targets from each scan position - this process took up the bulk of the time taken at each scan position. Replacing the Riegl VZ-1000 used here with a TLS system which do not require targets for alignment (through use of differential GPS and an inertial measurement unit) would have permitted a significantly larger area to be surveyed. This would be due to time no longer being required to scan targets nor to roll them between survey phases.

7 Location of the archived data

The data will be archived in the Centre for Environmental Data Analysis (CEDA) archive. Discussions with CEDA are ongoing to determine how the data can be archived to ensure users have access to the data they need. We intend to make the raw TLS data (with scan position and global transformation matrices) available as well as the digital terrain model, digital surface model and canopy height model and a tiled version of the point cloud. Until the data has been archived by CEDA, it can be made available upon request from the University of Edinburgh.

8 Publications

Hancock (in prep). Evaluation of the shadowVox voxel-based radiative transfer model.

References

R. Essery. Large-scale simulations of snow albedo masking by forests. *Geophysical Research Letters*, 40(20):5521–5525, 2013. ISSN 1944-8007. doi: 10.1002/grl.51008.

S. Gulev, P. Thorne, J. Ahn, F. Dentener, C. Domingues, S. Gerland, D. Gong, D. Kaufman, H. Nnamchi, J. Quaas, J. Rivera, S. Sathyendranath, S. Smith, B. Trewin, K. von Schuckmann, and R. Vose. *Changing State of the Climate System*, page 287–422. Cambridge University Press, Cambridge, United Kingdom and New York, NY, USA, 2021. doi: 10.1017/9781009157896.004.

J. Hackenberg, H. Spiecker, K. Calders, M. Disney, and P. Raumonen. SimpleTree —An Efficient Open Source Tool to Build Tree Models from TLS Clouds. *Forests*, 6(11):4245–4294, Nov. 2015. doi: 10.3390/f6114245. Number: 11 Publisher: Multidisciplinary Digital Publishing Institute.

J. Malle, N. Rutter, G. Mazzotti, and T. Jonas. Shading by Trees and Fractional Snow Cover Control the Subcanopy Radiation Budget. *Journal of Geophysical Research: Atmospheres*, 124(6): 3195–3207, 2019. ISSN 2169-8996. doi: 10.1029/2018JD029908. _eprint: https://agupubs.onlinelibrary.wiley.com/doi/pdf/10.1029/2018JD029908.

G. Mazzotti, C. Webster, R. Essery, and T. Jonas. Increasing the Physical Representation of Forest-Snow Processes in Coarse-Resolution Models: Lessons Learned From Upscaling Hyper-Resolution Simulations. *Water Resources Research*, 57(5):e2020WR029064, 2021. ISSN 1944-7973. doi: 10.1029/2020WR029064. _eprint: https://onlinelibrary.wiley.com/doi/pdf/10.1029/2020WR029064.

W. Ni-Meister and H. Gao. Assessing the impacts of vegetation heterogeneity on energy fluxes and snowmelt in boreal forests. *Journal of Plant Ecology*, 4(1-2):37–47, Mar. 2011. ISSN 1752-9921. doi: 10.1093/jpe/rtr004.

Steven Hancock. voxelate, 2021. URL `https://bitbucket.org/StevenHancock/voxelate/src/master/`.

C. Webster, N. Rutter, F. Zahner, and T. Jonas. Modeling subcanopy incoming longwave radiation to seasonal snow using air and tree trunk temperatures. *Journal of Geophysical Research: Atmospheres*, 121(3):1220–1235, 2016. ISSN 2169-8996. doi: 10.1002/2015JD024099.

Table 2: List of scan position locations with easting and northing in UTM32N (EPSG:32632) and elevation above the WGS84 ellipsoid (continued overleaf).

Scan Position	Easting (m)	Northing (m)	Elevation (m)
ScanPos001	566643.54	5188307.11	1585.29
ScanPos002	566643.32	5188307.03	1585.06
ScanPos003	566617.45	5188281.58	1583.81
ScanPos004	566617.67	5188281.49	1583.59
ScanPos005	566610.69	5188249.81	1585.06
ScanPos006	566610.84	5188249.97	1584.83
ScanPos007	566629.49	5188251.68	1584.64
ScanPos008	566629.67	5188251.76	1584.40
ScanPos009	566636.83	5188243.11	1585.33
ScanPos010	566636.67	5188243.25	1585.10
ScanPos011	566645.12	5188254.70	1584.44
ScanPos012	566645.00	5188254.89	1584.22
ScanPos013	566654.33	5188288.22	1584.11
ScanPos014	566654.37	5188288.26	1583.88
ScanPos015	566656.98	5188254.39	1585.34
ScanPos016	566657.21	5188254.37	1585.13
ScanPos017	566653.64	5188242.47	1584.35
ScanPos018	566653.77	5188242.28	1584.13
ScanPos019	566670.79	5188242.56	1583.50
ScanPos020	566670.89	5188242.60	1583.27
ScanPos021	566673.67	5188273.02	1583.45
ScanPos022	566673.77	5188272.81	1583.24
ScanPos023	566697.87	5188237.72	1581.66
ScanPos024	566742.16	5188227.37	1577.69
ScanPos025	566742.20	5188227.57	1577.46
ScanPos026	566658.53	5188314.53	1584.35
ScanPos027	566658.64	5188314.37	1584.11
ScanPos028	566674.47	5188318.50	1581.69
ScanPos029	566674.60	5188318.67	1581.46
ScanPos030	566680.80	5188310.26	1580.87
ScanPos031	566681.01	5188310.18	1580.66
ScanPos032	566690.10	5188295.02	1580.78
ScanPos033	566689.99	5188294.84	1580.55
ScanPos034	566693.56	5188303.14	1579.58
ScanPos035	566693.33	5188303.10	1579.37
ScanPos036	566703.92	5188303.09	1577.87
ScanPos037	566703.84	5188303.10	1577.64
ScanPos038	566706.89	5188281.57	1577.94
ScanPos039	566706.72	5188281.69	1577.71
ScanPos040	566717.58	5188267.96	1577.39
ScanPos041	566717.51	5188268.02	1577.17
ScanPos042	566729.98	5188256.85	1577.91
ScanPos043	566729.85	5188256.79	1577.68
ScanPos044	566735.00	5188237.16	1577.72
ScanPos045	566734.80	5188237.12	1577.50
ScanPos046	566734.82	5188272.29	1578.11
ScanPos047	566734.62	5188272.39	1577.89
ScanPos048	566742.60	5188299.21	1576.85
ScanPos049	566718.02	5188313.88	1578.42
ScanPos050	566718.10	5188313.69	1578.19

Scan Position	*Easting (m)*	*Northing (m)*	*Elevation (m)*
ScanPos051	566691.82	5188318.33	1579.00
ScanPos052	566691.79	5188318.54	1578.76
ScanPos053	566682.84	5188325.09	1579.46
ScanPos054	566682.98	5188325.25	1579.23
ScanPos055	566670.39	5188332.52	1580.98
ScanPos056	566670.49	5188332.71	1580.75
ScanPos057	566677.72	5188347.43	1580.03
ScanPos058	566677.90	5188347.37	1579.79
ScanPos059	566692.24	5188339.96	1577.45
ScanPos060	566692.02	5188340.03	1577.24
ScanPos061	566692.68	5188355.99	1579.40
ScanPos062	566692.80	5188355.82	1579.17
ScanPos063	566704.32	5188374.78	1582.05
ScanPos064	566704.45	5188374.60	1581.82
ScanPos065	566713.95	5188380.43	1582.64
ScanPos066	566714.04	5188380.24	1582.42
ScanPos067	566708.58	5188358.31	1579.00
ScanPos068	566708.57	5188358.10	1578.77
ScanPos069	566722.50	5188361.48	1578.83
ScanPos070	566722.30	5188361.39	1578.61
ScanPos071	566722.34	5188345.29	1577.56
ScanPos072	566722.16	5188345.16	1577.34
ScanPos073	566743.88	5188376.30	1577.79
ScanPos074	566743.87	5188376.52	1577.54
ScanPos075	566760.26	5188372.13	1577.62
ScanPos076	566760.12	5188371.96	1577.41
ScanPos077	566766.58	5188360.14	1577.88
ScanPos078	566766.51	5188359.93	1577.65
ScanPos079	566775.53	5188346.59	1576.33
ScanPos080	566775.36	5188346.45	1576.11
ScanPos081	566755.83	5188347.35	1577.81
ScanPos082	566755.62	5188347.38	1577.58
ScanPos083	566751.67	5188335.97	1577.64
ScanPos084	566751.68	5188335.89	1577.42
ScanPos085	566746.37	5188323.75	1576.89
ScanPos086	566746.15	5188323.78	1576.68
ScanPos087	566742.33	5188334.63	1578.36
ScanPos088	566742.30	5188334.42	1578.14
ScanPos089	566736.55	5188338.79	1578.45
ScanPos090	566736.40	5188338.94	1578.22
ScanPos091	566734.03	5188320.74	1577.20
ScanPos092	566733.91	5188320.95	1577.00
ScanPos093	566753.08	5188326.17	1576.49
ScanPos094	566753.07	5188325.95	1576.28
ScanPos095	566760.65	5188340.63	1576.30
ScanPos096	566760.85	5188340.55	1576.08
ScanPos097	566764.08	5188328.89	1576.36
ScanPos098	566764.10	5188328.82	1576.14
ScanPos099	566772.47	5188321.82	1576.96
ScanPos100	566772.41	5188321.60	1576.75

Continued overleaf

Scan Position	*Easting (m)*	*Northing (m)*	*Elevation (m)*
ScanPos101	566777.09	5188332.10	1576.65
ScanPos102	566776.94	5188332.25	1576.42
ScanPos103	566772.10	5188335.49	1576.54
ScanPos104	566772.09	5188335.55	1576.32
ScanPos105	566780.72	5188337.78	1576.46
ScanPos106	566780.93	5188337.78	1576.24
ScanPos107	566788.06	5188337.32	1576.39
ScanPos108	566787.84	5188337.34	1576.16
ScanPos109	566795.45	5188331.72	1578.64
ScanPos110	566795.24	5188331.70	1578.41
ScanPos111	566797.05	5188319.43	1579.32
ScanPos112	566796.82	5188319.43	1579.11
ScanPos113	566795.92	5188308.63	1578.24
ScanPos114	566796.15	5188308.68	1578.02
ScanPos115	566798.28	5188295.81	1579.12
ScanPos116	566798.06	5188295.83	1578.89
ScanPos117	566786.75	5188295.66	1578.91
ScanPos118	566786.58	5188295.51	1578.70
ScanPos119	566783.82	5188306.58	1577.47
ScanPos120	566783.66	5188306.42	1577.25
ScanPos121	566787.69	5188314.38	1577.59
ScanPos122	566787.73	5188314.60	1577.37
ScanPos123	566788.80	5188324.04	1576.79
ScanPos124	566788.87	5188323.83	1576.57
ScanPos125	566791.12	5188349.96	1576.15
ScanPos126	566790.97	5188349.80	1575.94
ScanPos127	566793.10	5188368.29	1575.83
ScanPos128	566793.11	5188368.11	1575.59
ScanPos129	566777.44	5188312.36	1577.98
ScanPos130	566777.32	5188312.25	1577.76
ScanPos131	566773.82	5188303.31	1578.09
ScanPos132	566773.70	5188303.52	1577.88
ScanPos133	566769.09	5188300.16	1578.24
ScanPos134	566768.87	5188300.12	1578.02
ScanPos135	566764.89	5188307.01	1577.64
ScanPos136	566765.09	5188307.10	1577.42
ScanPos137	566766.72	5188314.59	1576.90
ScanPos138	566766.67	5188314.52	1576.68
ScanPos139	566759.59	5188321.31	1576.69
ScanPos140	566759.41	5188321.20	1576.46
ScanPos141	566755.71	5188314.09	1576.90
ScanPos142	566755.52	5188313.99	1576.67
ScanPos143	566757.47	5188306.36	1576.99
ScanPos144	566757.66	5188306.45	1576.76
ScanPos145	566752.53	5188297.34	1577.20
ScanPos146	566752.62	5188297.53	1576.97
ScanPos147	566768.82	5188289.68	1577.83
ScanPos148	566768.89	5188289.87	1577.61
ScanPos149	566778.11	5188288.48	1578.44
ScanPos150	566778.12	5188288.39	1578.22

Continued overleaf

Scan Position	*Easting (m)*	*Northing (m)*	*Elevation (m)*
ScanPos151	566784.21	5188285.16	1578.10
ScanPos152	566784.02	5188285.28	1577.88
ScanPos153	566798.47	5188286.70	1578.89
ScanPos154	566798.27	5188286.75	1578.67
ScanPos155	566790.63	5188275.25	1578.00
ScanPos156	566790.44	5188275.32	1577.77
ScanPos157	566785.07	5188279.78	1578.77
ScanPos158	566784.85	5188279.77	1578.55
ScanPos159	566774.34	5188282.24	1578.38
ScanPos160	566774.40	5188282.02	1578.16
ScanPos161	566764.59	5188285.58	1577.89
ScanPos162	566764.81	5188285.62	1577.67
ScanPos163	566757.51	5188277.19	1578.04
ScanPos164	566757.65	5188277.04	1577.81
ScanPos165	566767.35	5188273.12	1578.10
ScanPos166	566767.14	5188273.09	1577.88
ScanPos167	566774.62	5188268.37	1578.13
ScanPos168	566774.61	5188268.14	1577.92
ScanPos169	566779.36	5188261.99	1577.81
ScanPos170	566779.17	5188262.10	1577.58
ScanPos171	566789.84	5188265.41	1577.45
ScanPos172	566789.65	5188265.52	1577.23
ScanPos173	566781.26	5188253.43	1577.51
ScanPos174	566781.16	5188253.63	1577.30
ScanPos175	566772.23	5188261.18	1577.74
ScanPos176	566772.14	5188260.98	1577.51
ScanPos177	566761.19	5188265.06	1577.85
ScanPos178	566761.42	5188265.12	1577.64
ScanPos179	566755.02	5188268.36	1577.79
ScanPos180	566755.02	5188268.15	1577.57
ScanPos181	566744.11	5188261.05	1578.31
ScanPos182	566744.09	5188261.27	1578.08
ScanPos183	566739.49	5188253.35	1578.14
ScanPos184	566739.69	5188253.48	1577.93
ScanPos185	566735.71	5188245.23	1577.88
ScanPos186	566735.93	5188245.28	1577.66
ScanPos187	566740.58	5188240.27	1577.73
ScanPos188	566740.74	5188240.39	1577.49
ScanPos189	566750.75	5188234.82	1577.55
ScanPos190	566750.81	5188235.04	1577.34
ScanPos191	566752.65	5188244.77	1577.88
ScanPos192	566752.67	5188244.99	1577.66
ScanPos193	566760.02	5188244.44	1577.84
ScanPos194	566759.86	5188244.32	1577.61
ScanPos195	566766.45	5188250.37	1577.62
ScanPos196	566766.24	5188250.44	1577.41
ScanPos197	566755.79	5188260.89	1577.96
ScanPos198	566755.82	5188261.11	1577.74
ScanPos199	566747.20	5188255.31	1577.99
ScanPos200	566747.19	5188255.55	1577.79

Continued overleaf

Scan Position	*Easting (m)*	*Northing (m)*	*Elevation (m)*
ScanPos201	566764.80	5188233.85	1577.22
ScanPos202	566764.60	5188233.94	1577.00
ScanPos203	566757.46	5188226.80	1577.20
ScanPos204	566757.46	5188227.03	1576.99
ScanPos205	566772.04	5188223.20	1578.69
ScanPos206	566772.19	5188223.35	1578.46
ScanPos207	566782.45	5188209.09	1579.04
ScanPos208	566782.53	5188209.28	1578.81
ScanPos209	566795.68	5188210.24	1579.17
ScanPos210	566795.52	5188210.36	1578.93
ScanPos211	566780.77	5188234.89	1578.88
ScanPos212	566780.85	5188235.10	1578.66
ScanPos213	566791.73	5188234.47	1580.04
ScanPos214	566791.55	5188234.61	1579.82
ScanPos215	566793.66	5188244.79	1578.71
ScanPos216	566793.54	5188244.99	1578.50
ScanPos217	566800.99	5188237.50	1579.93
ScanPos218	566801.21	5188237.49	1579.72
ScanPos219	566810.05	5188244.14	1579.80
ScanPos220	566809.82	5188244.11	1579.58
ScanPos221	566800.47	5188253.95	1578.95
ScanPos222	566800.32	5188254.14	1578.76
ScanPos223	566800.91	5188264.27	1579.41
ScanPos224	566800.99	5188264.06	1579.19
ScanPos225	566814.52	5188261.59	1580.26
ScanPos226	566814.32	5188261.67	1580.03